Int. Journal of Refractory Metals and Hard Materials 41 (2013) 522–530

Contents lists available at ScienceDirect

Int. Journal of Refractory Metals and Hard Materials

journal homepage: www.elsevier.com/locate/IJRMHM

The relationship between microstructure and fracture toughness of zirconia toughened alumina (ZTA) added with MgO and CeO_2

Nik Akmar Rejab [a], Ahmad Zahirani Ahmad Azhar [a], Mani Maran Ratnam [b], Zainal Arifin Ahmad [a,*]

[a] Structural Materials Niche Area, School of Materials and Mineral Resources, Engineering Campus, Universiti Sains Malaysia, 14300 Nibong Tebal, Penang, Malaysia
[b] School of Mechanical Engineering, Engineering Campus, Universiti Sains Malaysia, 14300 Nibong Tebal, Penang, Malaysia

ARTICLE INFO

Article history:
Received 22 February 2013
Accepted 17 July 2013

Keywords:
Microstructure
Vickers hardness
Fracture toughness
Palmqvist crack

ABSTRACT

The aim of this research is to investigate the mode of crack propagation in zirconia toughened alumina (ZTA) added with MgO and CeO_2, respectively. The mode of crack refers to the toughening mechanism of the materials. Different ZTA compositions containing MgO and CeO_2 as sintering additives were prepared using pressureless sintering at 1600 °C. Each sample was subjected to Vickers indentation with 294 N load and the cracks that propagated were observed with SEM. The ZTA with an addition of 0.7 wt.% MgO showed a crack deflection with a fracture toughness value of 6.19 ± 0.26 MPa · √m. On the other hand, the ZTA with CeO_2 addition of 0.5 to 7 wt.% showed both crack bridging and deflection, and produced 5.78 ± 0.16 MPa · √m to 6.59 ± 0.23 MPa · √m fracture toughness values, respectively. The fracture toughness of the ZTA–MgO–CeO_2 compositions is higher due to crack bridging and crack deflection. The toughening mechanisms of crack deflection and bridging hinder crack propagation since more energy is required to make the crack propagate. However, the formation of $CeAl_{11}O_{18}$ phase was observed; this consequently decreases the hardness and fracture toughness of the ZTA–MgO–CeO_2 compositions.

1. Introduction

Al_2O_3 can be considered as an all-rounded material for engineering ceramics. The properties of this ceramic are particularly attractive for structural applications such as in motor, aerospace, and biomedical fields, especially in severe environmental conditions [1]. Brittleness and poor damage tolerance have limited the scope of use as advanced engineering materials for almost all composition materials [2]. The fracture toughness of composition materials is generally low because the dislocation motion in the material is extremely limited due to the nature of the chemical bonds which are ionic and/or covalent. The problem of low fracture toughness in the ceramics can be overcome by designing and preparing the composite materials reinforced with fibers, whiskers, and particulates of the same phase as that of the matrix or of a different but suitable phase. The use of ZrO_2-based ceramics is one of the possible alternatives to circumvent the limitation of low fracture toughness [3,4].

In spite of the variety of useful physical properties of sintered oxide ceramics that are based on chemically and thermally stable modification of α-Al_2O_3, their application as cutting tool inserts working under mechanical loads and thermal shock conditions is limited due to their brittleness and low strength. To overcome the brittleness, reinforcement such as YSZ is introduced into Al_2O_3, producing zirconia toughened alumina (ZTA). YSZ increases the toughness by transforming the phase from $ZrO_{2(t)}$ to $ZrO_{2(m)}$ [5–7].

Zirconia toughened Al_2O_3 (ZTA) has been reported to be one of the most successful commercial ceramic-based cutting inserts which fully utilize the advantages of zirconia [2]. Recently, materials with certain intermetallic matrices were reported to may also benefit from the addition of zirconia particles. Dogan and Hawk applied 20 mass% of zirconia into $MoSi_2$ system which resulted in a 25–100% increase in fracture toughness of the material, depending upon which toughening mechanisms are activated.

Because strengthening increases linearly with the amount of tetragonal phase, zirconia with 100% of tetragonal phase gives the highest strength. In addition, zirconia with 100% of tetragonal phase is known as tetragonal zirconia polycrystals (TZP). The amount of oxide added must be limited so that the phase is still tetragonal during sintering. On the other hand, the amount must not be too small because the transformation of the tetragonal grains to the monoclinic state cannot be suppressed [8].

Previous works [9–14] have investigated the effects of various additives on the microstructural, mechanical properties, and tool wear of ZTA composites. Furthermore, their analysis has also proven that ZTA composite is an excellent candidate for cutting insert applications. However, their investigation on the toughness and crack behavior properties were not thorough as they only measured the fracture toughness of the composite, but did not observe and/or investigate the crack propagation behavior of their ceramic compositions.

* Corresponding author. Tel.: +60 4 5996128; fax: +60 4 5941011.
E-mail address: zainal@eng.usm.my (Z.A. Ahmad).

0263-4368/$ – see front matter © 2013 Elsevier Ltd. All rights reserved.
http://dx.doi.org/10.1016/j.ijrmhm.2013.07.002

Therefore, the influence of sintering additives, such as MgO and CeO_2 with different volume fractions on the microstructural characteristics, fracture toughness, and crack behavior of ZTA compositions was investigated. The fracture toughness and hardness of each sample were determined at room temperature. In addition, bulk density, Vickers hardness, and phase identification of the sintered samples which are also dependent on sintering additives were determined.

2. Materials and methodology

Starting powders of highly pure, thermally reactive type Al_2O_3 (Alcoa, A16SG, 99.0%), yttrium stabilized zirconia (Goodfellow, 94.6%), 20 nm MgO (Strem Chemicals, Inc., 99.9%), and CeO_2 (Sigma-Aldrich Corporation, 99.0%) were used. The particle size analysis of starting materials was carried out with Sympatec Nanophox (NX0064). In this work, 80 wt.% of Al_2O_3 and 20 wt.% yttrium stabilized zirconia were taken as the baseline composition. The amount of MgO was fixed at 0.7 wt.% due to its excellent hardness values [9]. The ceria were added in different wt.% (0.5 to 7 wt.%) into the initial compositions. Table 1 shows the addition in weight percentage (wt.%) for each powder composition used. The mixtures were prepared by the wet milling method. Subsequently, the mixtures were dried to 100 °C and crushed to form powders. Cylindrical shapes with dimensions of 13.0 mm in diameter and 4.0 mm in height were formed by pressing the crushed powder at 300 MPa. Afterwards, these cylindrical samples were sintered in atmosphere at 1600 °C for 4 h to yield dense ceramics.

The density and porosity values were obtained according to the ASTM C 830-00 test procedure. The analysis of crystal structure was carried out by X-ray diffraction (XRD) using the Bruker D8 Advance with CuKa radiation (40 kV, 30 mA) diffracted beam monochromator, using a step scan mode with a step size of 0.1° in the range of 20°–80° of 2θ°. Scanning electron microscopy (SEM) was employed to study the microstructure of the polished samples. The IMT iSolution DT software was used to discriminate and measure the percentage of each phase from the SEM microstructure. The fracture toughness, which is a critical mechanical property parameter in this work, was determined by the indentation technique. The samples were carefully diamond-polished to produce an optical finish. In the indentation test (Shimadzu Vickers hardness tester HSV-20, Japan), a 294 N load was applied by pressing the indenter onto the sample surface. Both the diagonal length of the indentation and crack length were measured. 10 indent points were made for each sample and the average was taken. K_{1C}(HV30) was calculated using Eq. (1) [15]:

$$3K_{Ic} = 0.035\left(Ha^{1/2}\right)(3E/H)^{0.4}(l/a)^{-0.5} \quad (1)$$

where K_{1C} is the fracture toughness, H is Vickers hardness, a is the half length of Vickers diagonal (μm), E is the Young modulus of the samples, and l is the length of the radial crack size (μm). Young modulus for all the samples was determined using rules of mixtures and calculated with respect to the composition of each sample.

Table 1
Addition of CeO_2 in weight percentage (wt.%) for each composition.

Sample	ZTA	MgO (wt.%)	CeO_2 (wt.%)
ZTA*	100	0.0	0.0
ZTA–MgO	99.3	0.7	0.0
ZTA–MgO–0.5CeO_2	98.8	0.7	0.5
ZTA–MgO–0.7CeO_2	98.6	0.7	0.7
ZTA–MgO–1.0CeO_2	98.3	0.7	1.0
ZTA–MgO–5.0CeO_2	94.3	0.7	5.0
ZTA–MgO–7.0CeO_2	92.3	0.7	7.0

* Composition of all ZTA was fixed to 80 wt.% Al_2O_3 and 20 wt.% YSZ.

3. Results and discussion

Fig. 1 shows the average particle size, particle size distribution, and morphology for all of the raw powders used. The average particle sizes for Al_2O_3 and YSZ were 1.05 μm and 0.71 μm, while the MgO nano particle and CeO_2 powder were 18.35 nm and 138.69 nm, respectively. Table 2 summarizes the overall results for grain size, Vickers hardness, fracture toughness, theoretical density, bulk density, and porosity. The comparison of crack propagation between pure Al_2O_3 and ZTA is shown in Fig. 2. The scanning electron microscope (SEM) micrographs of the indentation show cracks emanating from the corners of the Vickers indentation. The crack mode for both samples resulted in some crack deflections, as indicated by the white arrows at the Al_2O_3 and YSZ grains. However, the propagated crack experienced less deflection in pure Al_2O_3 compared to ZTA; the crack directly propagated through these grains, showing transgranular tendency. ZTA samples show more crack deflection due to the presence of $t \rightarrow m$ phase transformation during the crack propagation. A similar observation was reported by previous authors [16,17]. The behavior of crack propagation for Al_2O_3 would suggest that Al_2O_3 fracture toughness is lower compared to ZTA. The values of fracture toughness for Al_2O_3 and ZTA are 2.85 ± 0.40 MPa · √m and 4.42 ± 0.35 MPa · √m, respectively. Although sintered Al_2O_3 shows a larger grain size (4.30 ± 3.00 μm) compared to ZTA, their fracture toughness was reported to be lower [11].

Fig. 3 shows the indentation profile for the sample ZTA–MgO with 0 wt.% CeO_2. An enlarged view of one crack path is shown in an inset in Fig. 3. The crack path, as can be seen in the inset, indicates the crack propagation with associated crack deflection behavior on the surface. Fig. 4 (a)–(b) shows the surface morphology of cracks for samples ZTA–MgO and ZTA–MgO–0.7 wt.% CeO_2, respectively. The crack deflection can be observed under indentation load of 294 N. The fracture toughness value for ZTA–MgO–0 wt.% CeO_2 (baseline sample) and ZTA–MgO–1.0 wt.% CeO_2 were 5.75 ± 0.33 MPa · √m and 6.59 ± 0.23 MPa · √m, respectively. ZTA–MgO–1.0 wt.% CeO_2 has higher fracture toughness due to a higher number of crack deflections found on the crack propagation compared to a sample of ZTA–MgO–0 wt.% CeO_2, as shown in Fig. 4. With the presence of CeO_2, ZTA–CeO_2 samples show more crack deflection due to Al_2O_3 strengthening by CeO_2 [14].

Besides the modes of crack propagation in ZTA, the presence of YSZ in the Al_2O_3 clearly contributed to the increase of fracture toughness. XRD spectra of the ZTA–MgO–CeO_2 compositions sintered at 1600 °C for 4 h are shown in Fig. 5. From the XRD patterns, it is observed that the major diffraction peaks can be indexed as yittria doped zirconia ($Zr_{0.935}Y_{0.065})O_{1.968}$ (designated as ^{O}, ICDD files No. 01-078-1808), and α-Al_2O_3 (designated as □, ICDD files No. 00-010-0173). Three minor phases were also identified, i.e., m-ZrO_2 (designated as *, ICDD files No. 01-078-1807), $MgAl_2O_4$ (designated as ◊, ICDD files No. 01-073-1959), and $CeAl_{11}O_{18}$ (designated as Δ, ICDD files No. 00-048-0055). Various literatures [1,8,18,19] suggest that the transformation toughening inside ZTA is an efficient mechanism that improves the toughness of ceramic composites containing YSZ. Furthermore, addition of CeO_2 also acts as a stabilizing agent. XRD results in Fig. 5 show that the peak for the monoclinic phase decreases with increased addition of CeO_2. The reduction of the monoclinic phase resulted in the increase of the tetragonal phase, thus promoting more transformation toughening $t \rightarrow m$ in ZTA ceramic composites. The addition of CeO_2 also decreases the monoclinic phase, as shown at 28° and 32° Bragg angles. Previous work done by Huang et al., who studied the reduction of CeO_2 in ZrO_2 ceramics, also shows a reduction of the monoclinic phase with the addition of CeO_2 [20]. The reduction of the monoclinic phase in ZTA–MgO–CeO_2 system increases the overall toughness of the ceramic composite. This is due to the presence of more tetragonal ZrO_2, which promotes the transformation toughening mechanism. A similar observation was also reported by Azhar et al. and Rejab et al. on the ZTA–Cr_2O_3 system where the presence of Cr_2O_3 can be used to lower the presence of the monoclinic phase. The presence of monoclinic zirconia phase was an unavoidable

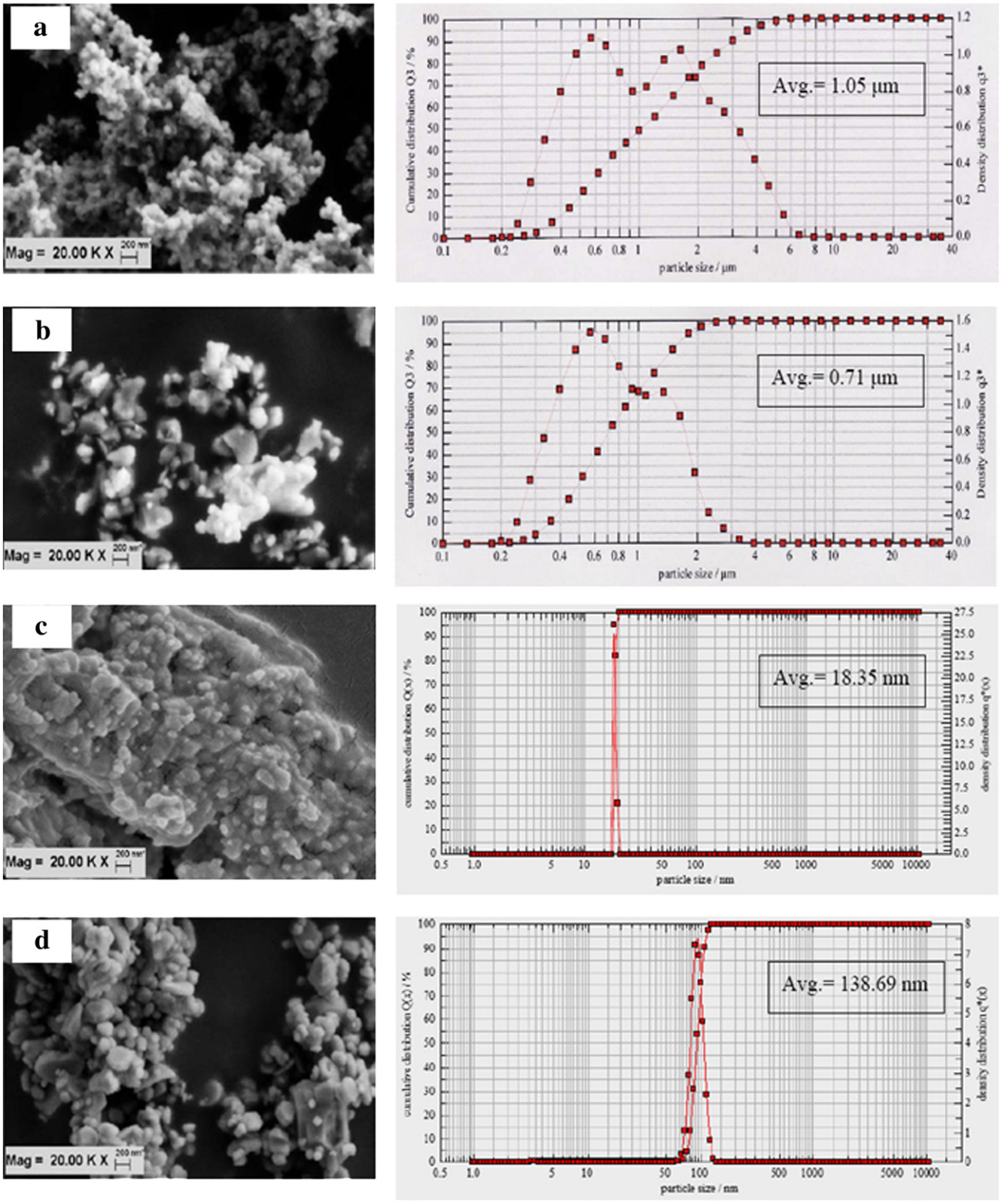

Fig. 1. The average particle size, particle size distribution and morphology for all of the raw powders used (a) Al_2O_3, (b) YSZ, (c) MgO-nano, and (d) CeO_2.

phenomenon and the small amount of monoclinic ZrO_2 would not affect the mixture as a whole. Sergo et al. reported that at least 15% of monoclinic phase will always be present, even in zirconia toughened alumina (ZTA) commercial cutting tools [21]. The presence of $MgAl_2O_4$ phase was first detected for ZTA–MgO without CeO_2 addition (Fig. 5b). The $MgAl_2O_4$ peaks were more apparent at the Bragg angle of 37.02°, as shown in Fig. 5. An image analyzer proved that the percentage area of $MgAl_2O_4$ phase at 0.5 to 1.0 wt.% CeO_2 addition was diminished from

Table 2
Physical and mechanical properties of ZTA–MgO with various amounts of CeO_2 addition.

Composition	Grain size (μm)		Hardness (GPa)	Fracture toughness (MPa · √m)	Theoretical density (g/m^3)	Bulk density (g/m^3)	Porosity (%)
	YSZ	Al_2O_3					
ZTA	1.21 ± 0.30	2.67 ± 0.45	15.30 ± 0.28	5.75 ± 0.33	4.40	4.13	1.66
ZTA–MgO	1.48 ± 0.28	2.14 ± 0.82	14.31 ± 0.15	5.77 ± 0.15	4.43	4.18	3.05
ZTA–MgO–0.5CeO_2	1.57 ± 0.34	2.88 ± 0.54	14.62 ± 0.22	5.78 ± 0.16	4.47	4.21	2.32
ZTA–MgO–0.7CeO_2	1.65 ± 0.60	2.94 ± 0.69	14.83 ± 0.27	6.19 ± 0.26	4.48	4.25	0.45
ZTA–MgO–1.0CeO_2	1.67 ± 0.37	2.95 ± 0.63	14.99 ± 0.31	6.59 ± 0.23	4.50	4.28	0.48
ZTA–MgO–5.0CeO_2	1.89 ± 0.41	2.98 ± 0.56	14.52 ± 0.23	5.72 ± 0.25	4.79	4.25	0.42
ZTA–MgO–7.0CeO_2	1.91 ± 0.46	2.86 ± 0.49	14.15 ± 0.19	5.58 ± 0.20	4.94	4.27	1.62

3.31 to 1.73%. Further addition of 5.0 to 7.0 wt.% CeO_2 caused the $MgAl_2O_4$ peaks to disappear and the new phase formation of $CeAl_{11}O_{18}$ to appear.

The addition of 5.0 wt.% and 7.0 wt.% of CeO_2 resulted in the formation of $CeAl_{11}O_{18}$. This is shown in the Bragg angle of 29°–37° in Fig. 5. The presence of $CeAl_{11}O_{18}$ could be due to solubility limits being exceeded because of excessive CeO_2 addition in the ZTA–MgO compositions. According to the literature, the excess Ce^{4+} in the ZTA–MgO compositions form minority phases or segregate from the interior grain and move into the perovskite lattice, as observed by other authors [20,22]. The presence of the $CeAl_{11}O_{18}$ phase could affect the toughening mechanism. Akin et al. reported that the $CeAl_{11}O_{18}$ phase formation is associated with a reduction of CeO_2 to Ce_2O_3 and a reaction with Al_2O_3 at higher temperatures of around 1200–1400 °C [22]. The formation of the $CeAl_{11}O_{18}$ phase could be related to the reduction of CeO_2 to Ce_2O_3 and a reaction with Al_2O_3 at higher temperatures of around 1200–1400 °C, according to the following equation [22];

$$Ce_2O_3 + 11Al_2O_3 \rightarrow Ce_2O_3 \cdot 11Al_2O_3. \quad (2)$$

Fig. 6 shows the area percentages of each phase in the ZTA–MgO–CeO_2 composites. The $CeAl_{11}O_{18}$ phase started to appear at 1 wt.% and kept increasing until 7 wt.% CeO_2 addition, i.e., from 17.28% to 47.66%. The increase of $CeAl_{11}O_{18}$ phase reduced the toughness of the sample. At the same time, the percentage of yttria doped zirconia $\{(Zr_{0.935}Y_{0.065})O_{1.968}\}$ phase (tetragonal structure) decreased from 18.35% to 12.36%. Therefore, due to the loss of this tetragonal phase in YSZ, the toughness also decreases. Table 3 shows the results of phase percentage area of each ZTA–MgO–CeO_2 composite. It is proven that the addition of CeO_2 does reduce the tetragonal phase; hence, the decrease of fracture toughness is due to the loss of tetragonal phase. The percentage of yittria doped zirconia $(Zr_{0.935}Y_{0.065})O_{1.968}$ phase (tetragonal structure) dropped from 18.35% to 12.36%. The highest reduction recorded for α-Al_2O_3 (corundum) was from 81.71% to 38.54%. High phase percentage reduction for α-Al_2O_3 refers to the presence of residual stress which is shown through some shifting in α-Al_2O_3 and YSZ peaks that were observed due to CeO_2 addition. The XRD peak shift occurred due to the presence of residual stress as the ionic radii for Ce^{4+} (0.96) and Al^{3+}(0.51) and differs significantly in the case of a substitutional solid solution. The stress relieved

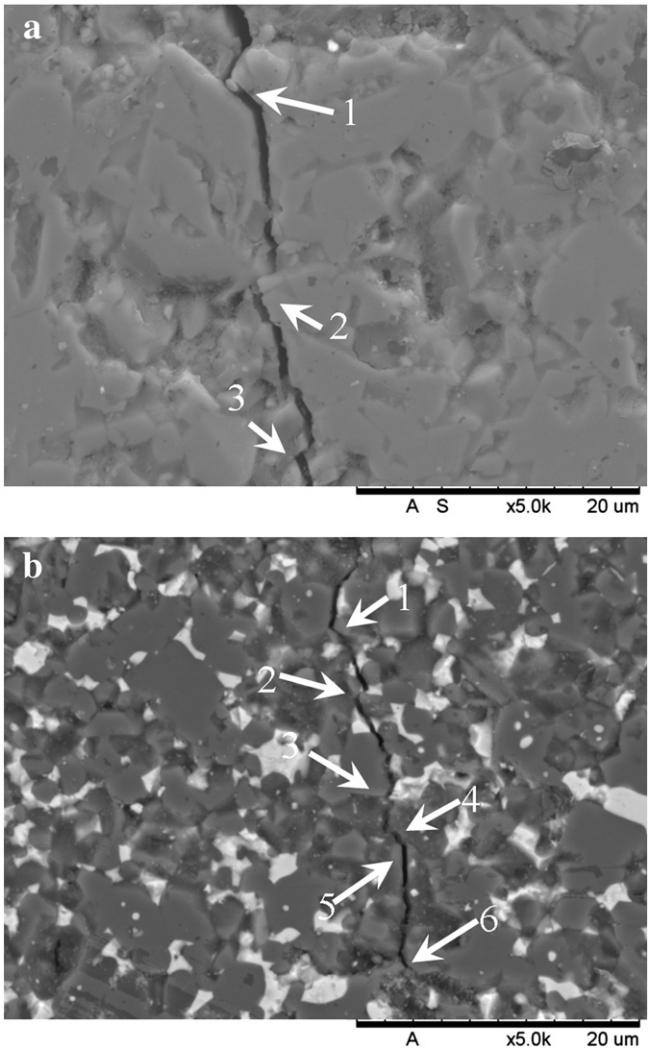

Fig. 2. Crack deflection comparison between (a) pure Al_2O_3, and (b) ZTA composite sintered at 1600 °C for 4 h. Crack propagation is downward.

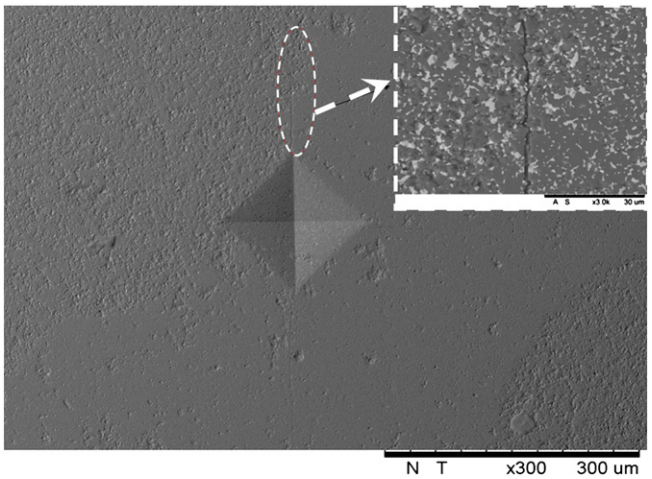

Fig. 3. The SEM micrograph of indent under a load of 294 N for sample ZTA–MgO without addition of CeO_2.

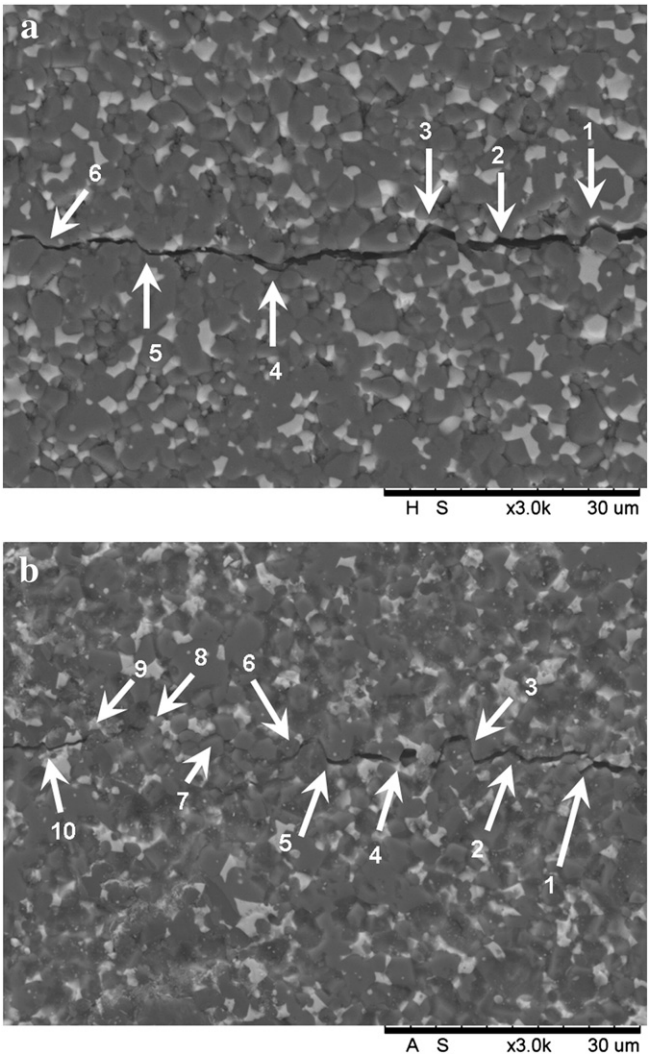

Fig. 4. Crack path in the (a) ZTA–MgO without CeO_2 and (b) ZTA–MgO–1.0 wt.% CeO_2, induced by Vickers indentation. Arrows indicate that major toughening mechanisms are crack deflection.

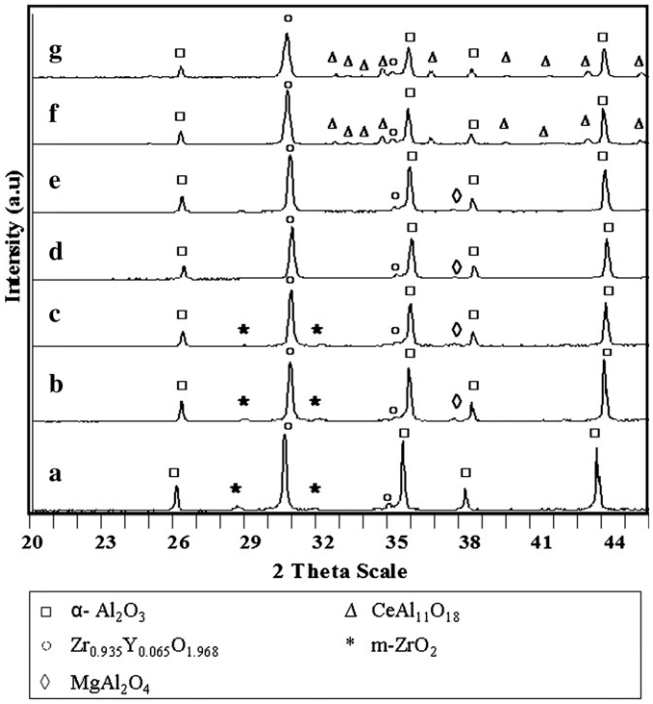

Fig. 5. XRD patterns of (a) ZTA, (b) ZTA–MgO, (c) ZTA–MgO–0.5 wt.% CeO_2, (d) ZTA–MgO–0.7 wt.% CeO_2, (e) ZTA–MgO–1 wt.% CeO_2, (f) ZTA–MgO–5 wt.% CeO_2, and (g) ZTA–MgO–7 wt.% CeO_2.

from the sintering process contributed to the peak shifting in the XRD pattern of ZTA–MgO–CeO_2 composites.

The crack propagation behavior of ZTA–MgO–CeO_2 composites are known to affect the fracture toughness of the samples [19]. The results for fracture toughness and Vickers hardness are shown in Fig. 7. The results of fracture toughness increased from 5.75 ± 0.33 MPa · √m to 6.59 ± 0.23 MPa · √m with the addition of 1.0 wt.% of CeO_2. According to the XRD pattern (Fig. 5), addition of CeO_2 reduces the monoclinic phase, as shown at 28° and 32° Bragg angles. Due to the disappearance of the monoclinic phase, the fracture toughness of the ZTA sample increased from 5.75 MPa · √m to 6.59 MPa · √m with the addition of 1.0 wt.% of CeO_2. Furthermore, the increment in the intrinsic toughness of alumina matrix and toughening mechanism introduced by zirconia particles as transformation toughening ($t \rightarrow m$) also contributed to the increase in fracture toughness. However, secondary phase ($CeAl_{11}O_{18}$) was detected at 5.0 wt.% and 7.0 wt.% of CeO_2 addition which decreased the fracture toughness to 5.72 ± 0.25 MPa · √m (5.0 wt.% of CeO_2) and 5.58 ± 0.20 MPa · √m (7.0 wt.% of CeO_2), respectively. The sample with 1.0 wt.% CeO_2 addition showed the highest value which is 6.59 ± 0.23 MPa · √m. The increase of the fracture toughness of the ZTA–MgO–CeO_2 compositions, as compared to the ZTA compositions, is obvious from the presence of crack deflection and bridging. Both cracks brought about by the crack diffusion process absorb the fracture energy and inhibit cracks from expanding to improve fracture toughness [23]. The result of Vickers hardness increased from 14.51 GPa to 14.99 GPa with the addition of 1.0 wt.% CeO_2. However, the addition of more CeO_2 led to a decrease in Vickers hardness values, from 14.99 GPa to 14.15 GPa. The decrease of Vickers hardness is possibly due to the presence of secondary phase of $CeAl_{11}O_{18}$. Theoretically, polycrystalline materials with finer grain size would give higher Vickers hardness while materials with coarser grain size will give higher values of fracture toughness. In the current study, it was found that ZTA with 1.0 wt.% of CeO_2 gave the highest Vickers hardness due to the maximum bulk density obtained (4.28 g/cm^3). The trend of Vickers hardness increased along with the results of bulk density only up to 1.0 wt.% of CeO_2. However, further addition of CeO_2 caused the bulk density to decrease due to the presence of secondary phase $CeAl_{11}O_{18}$. The decrease of bulk density led to the decrease of Vickers hardness. For fracture toughness, the trend showed an increase until 1.0 wt.% of CeO_2. The increase is attributed to the increase of Al_2O_3 grain size with further addition of CeO_2. According to the grain size measurements in Fig. 8, it can be stated that CeO_2 additions of 0.5–7.0 wt.% efficiently promoted grain growth of Al_2O_3. However, when the addition of CeO_2 was 5 wt.% and above, $CeAl_{11}O_{18}$ phase started to form and caused a decrease in the composite fracture toughness.

The appearance of $CeAl_{11}O_{18}$ is significant because it affects the fracture toughness and Vickers hardness of the ZTA–MgO–CeO_2 composites. The presence of $CeAl_{11}O_{18}$ is confirmed by the representative micrographs of ZTA–MgO–CeO_2 samples shown in Fig. 9. The bright and dark contrast grains correspond to YSZ and Al_2O_3 grains, respectively. The size of Al_2O_3 grains was inhibited due to the presence of YSZ grains. A similar micrograph observation was also reported by Azhar et al. The appearance of small fine grain size of Al_2O_3 is known to increase the hardness of ceramic composites. According to the grain size measurements in Fig. 8, it can be stated that CeO_2 additions of 0.5–7.0 wt.% efficiently promote grain growth of Al_2O_3. Average grain size increased approximately 38% with the addition of 7.0 wt.% of CeO_2. In this range, the largest

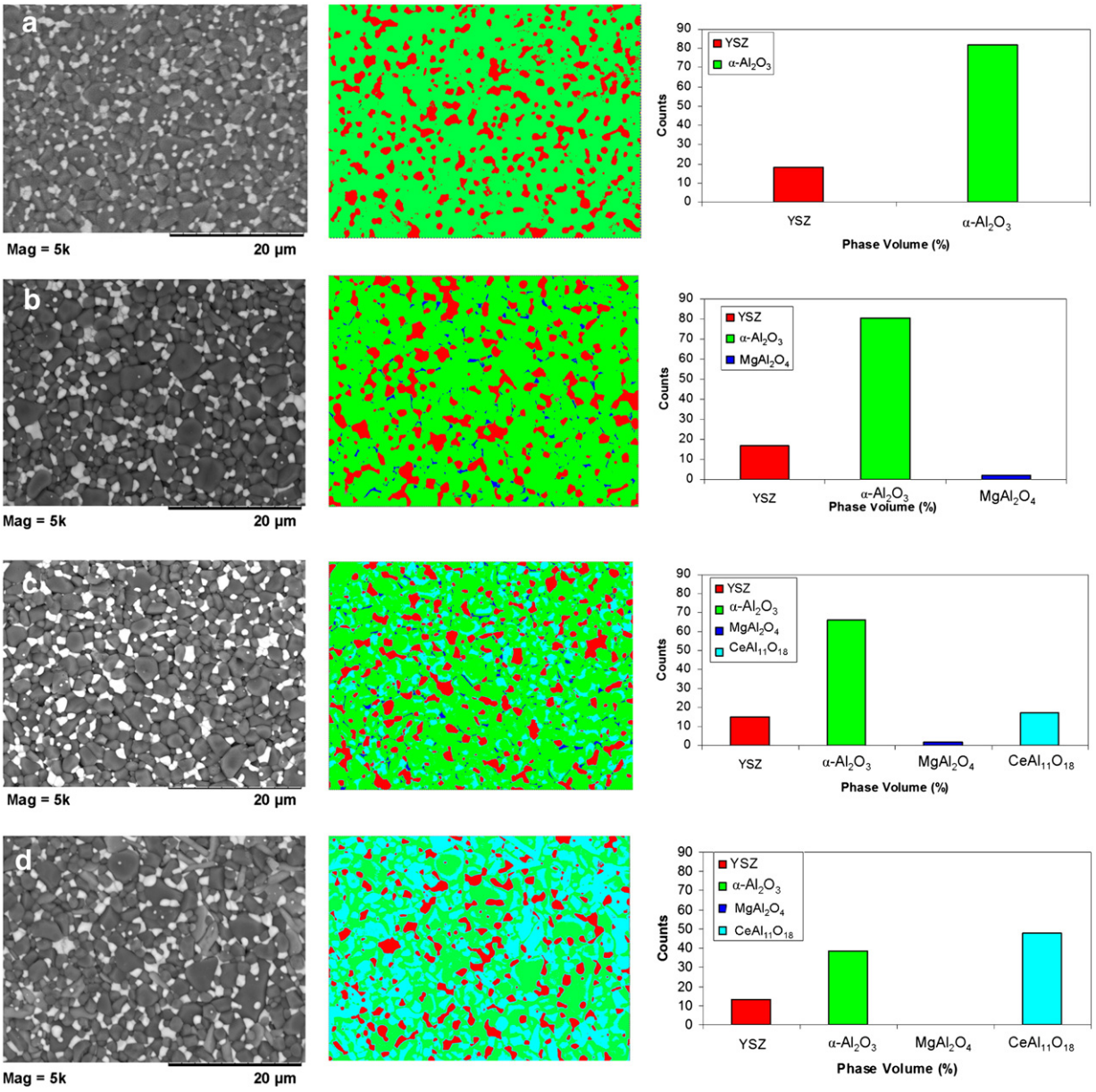

Fig. 6. Quantitative phase analysis of (a) ZTA, (b) ZTA–MgO, (c) ZTA–MgO–1.0 wt.% CeO_2, and (d) ZTA–MgO–7.0 wt.% CeO_2 based on their respective micrograph.

average grain size for Al_2O_3 obtained was the one corresponding to the sample with 5.0 wt.% (2.98 ± 0.56 μm); the smallest average grain size was obtained for the sample ZTA–MgO without CeO_2 addition (2.14 ± 0.82 μm). Furthermore, in the case of YSZ grains, the average grain size was (1.70 ± 0.41 μm) with increased CeO_2 additions. The formation of elongated grains of $CeAl_{11}O_{18}$ in the matrix of fine-grained Al_2O_3 was observed in the composites containing 5.0 and 7.0 wt.% CeO_2. Furthermore, the average length of $CeAl_{11}O_{18}$ grains was found to increase with the addition of CeO_2. The formation of $CeAl_{11}O_{18}$ promotes bonding between Al_2O_3 and CeO_2, which also has a contributing effect on the mechanical properties of the composite. Moreover, CeO_2 exhibits sensitivity to the sintering atmosphere and can form nonstoichiometric oxides such as Ce_2O_3 when sintering at low oxygen pressure atmosphere [22]. As shown in Fig. 9, the addition of CeO_2 above 5 wt.% clearly shows the formation of $CeAl_{11}O_{18}$ elongated grains. These elongated grains of $CeAl_{11}O_{18}$ tend to have larger grain sizes. The average size of elongated $CeAl_{11}O_{18}$ grains is 4–6 μm in length and 0.7–1 μm in width. The average length of elongated grains increased with increasing CeO_2 content from 5 wt.% (1.89 ± 0.41 μm) to 7 wt.% (1.91 ± 0.45 μm).

Table 3
Phase area percentage for each composition in ZTA–MgO–CeO_2 composites.

Composition	Phase area (%)			
	Al_2O_3	YSZ	$MgAl_2O_4$	$CeAl_{11}O_{18}$
ZTA	81.72	18.23	0.00	0.00
ZTA–MgO	78.87	17.12	3.31	0.00
ZTA–MgO–0.5CeO_2	76.15	18.39	4.43	0.00
ZTA–MgO–0.7CeO_2	80.56	16.65	2.09	0.00
ZTA–MgO–1.0CeO_2	66.07	14.80	1.73	17.28
ZTA–MgO–5.0CeO_2	52.02	12.83	0.00	30.88
ZTA–MgO–7.0CeO_2	38.54	13.08	0.00	47.66

Previous work done by Akin et al. also observed the formation of $CeAl_{11}O_{18}$ during spark plasma sintering (SPS) of Al_2O_3–YSZ–CeO_2 system. According to Akin et al., the presence of elongated $CeAl_{11}O_{18}$ grains

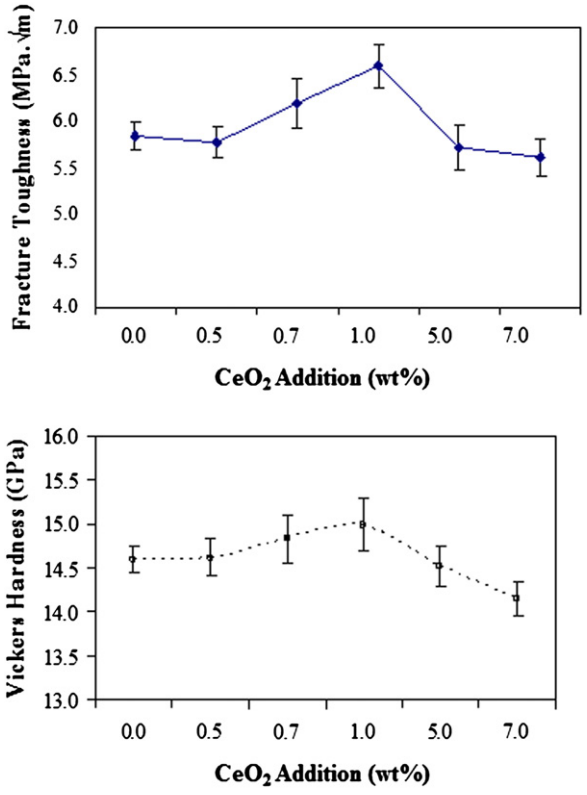

Fig. 7. Vickers hardness and fracture toughness of ZTA–MgO–CeO_2 compositions as a function of CeO_2 wt.%.

resulted in lower Vickers hardness and fracture toughness values compared to samples without the presence of $CeAl_{11}O_{18}$ grains. The Vickers hardness was reduced from 14.99 ± 0.31 GPa to 14.15 ± 0.19 GPa for samples with 1.0 wt.% CeO_2 to 7.0 wt.% CeO_2, respectively. The decrease of Vickers hardness is attributed to the change of Al_2O_3 grain size due to different CeO_2 content. In polycrystalline materials, samples with finer grain size will have higher Vickers hardness compared to polycrystalline materials with a larger grain size. This is due to the movement of dislocations between grains. These movements of dislocations provide a mechanism for planes of atoms to slip and results in plastic or permanent deformation. The movement allowed by these dislocations causes a decrease in the material's hardness. Furthermore, in polycrystalline materials, line defects or dislocations provide a mechanism for planes of atoms to slip, thus becoming a method for plastic or permanent deformation to happen. Planes of atoms can effectively flip from one side of the dislocation to the other, allowing the dislocation to traverse through the material and the material to deform permanently. The movement allowed by these dislocations causes a decrease in the material's hardness. When a dislocation intersects with a second dislocation, it can no longer traverse through the crystal lattice. The intersection of dislocations or crystal lattice with different arrangements of neighboring grains will create an anchor point and does not allow the planes of atoms to continue to slip over one another. For samples with finer grain size (ZTA–1.0 wt.% CeO_2), the movement of dislocations are restricted since the arrangement of crystal lattice is different to neighboring grains, creating more anchor points. Additional energy is required for the dislocation to traverse to neighboring grain, thus increasing the hardness.

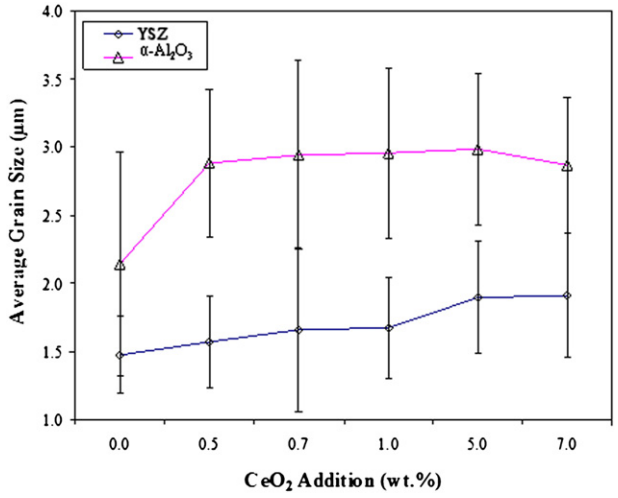

Fig. 8. Average grain size for both ZrO_2 and Al_2O_3 grains with varied CeO_2 addition in ZTA–MgO composites.

The density of all samples was measured by Archimedes' principle using water as the immersion medium. The theoretical density of the sample was determined based on the rule of mixtures (ROM) for the composite ceramics prepared. A theoretical density of approximately 99.0% was obtained for all ZTA–MgO and ZTA–MgO–CeO_2 compositions.

Fig. 10 shows the comparison of theoretical density and bulk density of sintered ZTA–MgO composite as a function of CeO_2 additions. The increment of bulk density values followed the theoretical values from 0.0 until 1.0 wt.% of CeO_2 additions. However, a decrease in bulk density was observed as the content of CeO_2 increased. The ZTA–MgO composition without CeO_2 addition showed a density of 4.18 g/cm^3. In samples with CeO_2 addition, densification was promoted and showed a maximum density at 1.0 wt.% of 4.28 g/cm^3. Further addition resulted in decreased density which corresponds to the presence of abnormal growth of elongated $CeAl_{11}O_{18}$ grains.

The Vickers hardness values were found to be highest in samples with the addition of 1.0 wt.% CeO_2. This is because the bulk densities observed were at maximum values (4.28 g/m^3) with 0.48% porosity and 6.59 ± 0.23 MPa · √m of toughness. The densities calculated for samples within the range of 0.0 to 1.0 wt.% of CeO_2 addition were in line/proportional with theoretical density. However, a contrary observation was found in samples with 5.0 to 7.0 wt.% of CeO_2 addition. It is suggested that the decrease is due to the presence of $CeAl_{11}O_{18}$ phase in ZTA–MgO ceramic. The addition of CeO_2 at certain wt.% (1.0–7.0 wt.%) in ZTA–MgO composites were found to have contributed to the formation of elongated grains ($CeAl_{11}O_{18}$) while the reduction in ZTA–MgO toughness and densities is due to changes in grain shape during coarsening [24]. Another factor that is closely related to density is porosity. Porosity is a defect which affects the density the most because porosity is inversely proportional to density. However, this is contradictory to author's [25] works. In addition, it is common for the porosity to increase with an increase in density. The addition of various amounts of CeO_2 (wt.%) densified ZTA–MgO composites (Fig. 10). Thus, from Fig. 10, it is believed that the presence of $CeAl_{11}O_{18}$ phases in ZTA–MgO–CeO_2 composites has critically influenced the density and porosity of the final product.

4. Conclusion

Toughened ZTA–MgO ceramics with different amounts of CeO_2 addition were prepared and then analyzed. The resulting microstructure differed in grain size and shape, depending on the amount of CeO_2 added. The crack propagation behavior corresponds to each microstructure change with respect to these characteristics. The ZTA sample with 0.7 wt.% MgO exhibited crack deflection with a fracture toughness value of 6.19 ± 0.26 MPa · √m. However, the compositions with CeO_2 addition of 0.5 to 1.0 wt.% showed increased crack bridging and deflection with fracture toughness ranging from 5.78 ± 0.16 MPa · √m to

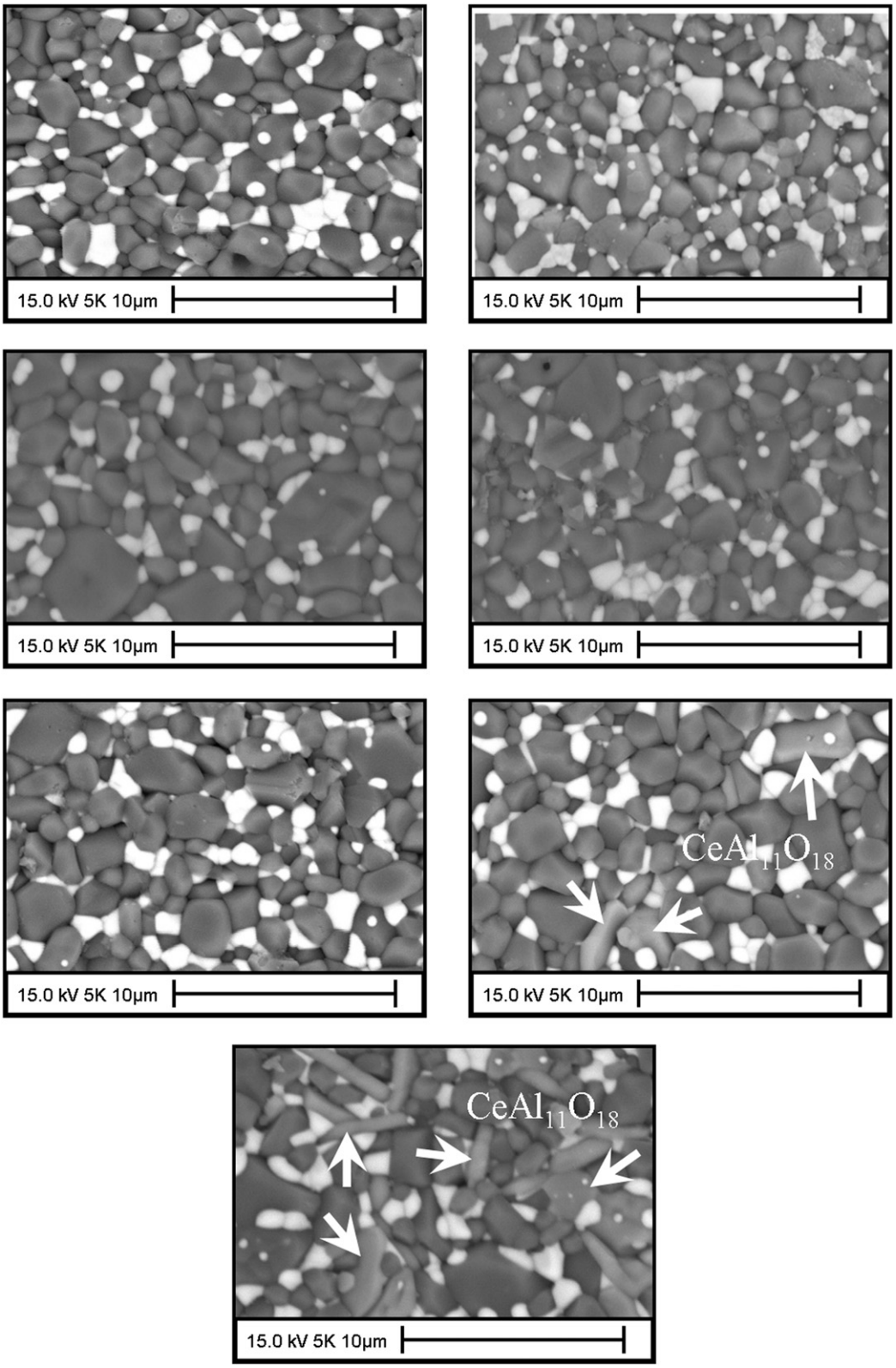

Fig. 9. SEM micrograph of the microstructure of ZTA and ZTA–MgO with CeO_2 addition (a) ZTA, (b) ZTA–MgO, (c) (c) ZTA–MgO–0.5 wt.% CeO_2, (d) ZTA–MgO–0.7 wt.% CeO_2, (e) ZTA–MgO–1.0 wt.% CeO_2, (f) ZTA–MgO–5.0 wt.% CeO_2, and (g) ZTA–MgO–7.0 wt.% CeO_2.

6.59 ± 0.23 MPa · √m. The addition of CeO_2 was found to significantly enhance both hardness and fracture toughness of ZTA–MgO composites. The Vickers hardness increased from 14.51 GPa to 14.99 GPa with the addition of 1.0 wt.% CeO_2, while the fracture toughness increased to 6.59 ± 0.23 MPa · √m with 1.0 wt.% CeO_2 addition. However, the presence of $CeAl_{11}O_{18}$ reduced the Vickers hardness and fracture toughness of the overall ceramics, which is in agreement with observations made by Akin et al. [22].

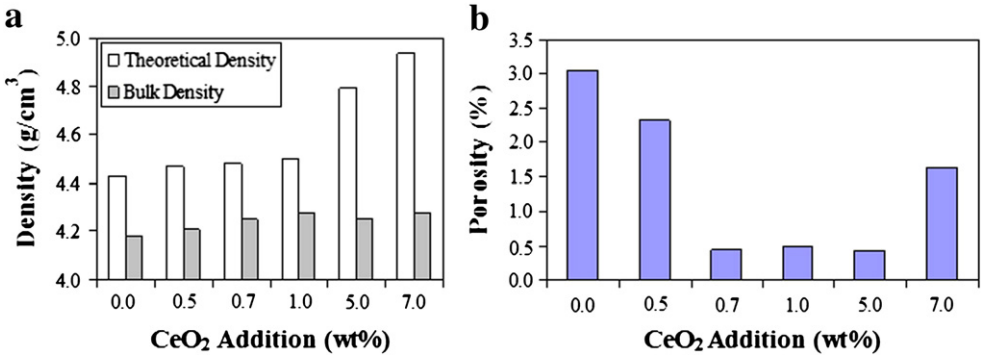

Fig. 10. Comparison of density of theoretical and bulk density for ZTA–MgO–CeO_2 compositions.

Acknowledgment

This work was funded by Universiti Sains Malaysia (USM) under grant 1001/PBAHAN/811212 and MyBrain15. The authors are grateful to Dr. Anasyida Abu Seman, Mr. Mokhtar Mohamad, Mr. Sharul Ami, Mr. Wan Fahmin, Mr. Khairi, and Mr. Abdul Rashid for their technical support.

References

[1] Cesari F, Esposito L, Furgiuele FM, Maletta C, Tucci A. Fracture toughness of alumina–zirconia composites. Ceram Int 2006;32:249–55.
[2] Maiti K, Sil A. Microstructural relationship with fracture toughness of undoped and rare earths (Y, La) doped Al_2O_3–ZrO_2 ceramic composites. Ceram Int 2011;37:2411–21.
[3] Kosmac T, Swain M, Claussen N. The role of tetragonal and monoclinic ZrO_2 particles in the fracture toughness of Al_2O_3–ZrO_2 composites. Mater Sci Eng 1985;71:57–64.
[4] Shukla S, Seal S, Vij R. Effect of nanocrystallite morphology on the metastable tetragonal phase stabilization in zirconia. Nano Lett 2002;2:989–93.
[5] Do an CP, Hawk JA. Role of zirconia toughening in the abrasive wear of intermetallic and ceramic composites. Wear 1997;212:110–8.
[6] Smuk B, Szutkowska M. Alumina ceramics with partially stabilized zirconia for cutting tools. J Mater Proc 2003;133:195–8.
[7] Szutkowska M. Fracture resistance behavior of alumina–zirconia composites. J Mater Process Technol 2004;153–154:868–74.
[8] Basu B, Vleugels J, Biest OVD. ZrO_2–Al_2O_3 composites with tailored toughness. J Alloys Compd 2004;372:278–84.
[9] Azhar AZA, Ratnam MM, Ahmad ZA. Effect of Al_2O_3/YSZ microstructures on wear and mechanical properties of cutting inserts. J Alloys Compd 2009;478:608–14.
[10] Azhar AZA, Mohamad H, Ratnam MM, Ahmad ZA. The effects of MgO addition on microstructure, mechanical properties and wear performance of zirconia-toughened alumina cutting inserts. J Alloys Compd 2010;497:316–20.
[11] Hao JKC, Azhar AZA, Ratnam MM, Ahmad ZA. Wear performance and mechanical properties of 80 wt.% Al_2O_3/20 wt.% YSZ cutting inserts at different sintering rates and soaking times. Mater Sci Technol 2010;26:95–103.
[12] Azhar AZA, Mohamad H, Ratnam MM, Ahmad ZA. Effect of MgO particle size on the microstructure, mechanical properties and wear performance of ZTA–MgO ceramic cutting inserts. Int J Refract Metals Hard Mater 2011;29:456–61.
[13] Azhar AZA, Choong LC, Mohamed H, Ratnam MM, Ahmad ZA. Effects of Cr_2O_3 addition on the mechanical properties, microstructure and wear performance of zirconia-toughened-alumina (ZTA) cutting inserts. J Alloys Compd 2012;513:91–6.
[14] Rejab NA, Azhar AZA, Ratnam MM, Ahmad ZA. The effects of CeO_2 addition on the physical, microstructural and mechanical properties of yttria stabilized zirconia toughened alumina (ZTA). Int J Refract Metals Hard Mater 2013;36:162–6.
[15] Niihara K. A fracture mechanics analysis of indentation-induced Palmqvist crack in ceramics. J Mater Sci Lett 1983;2:221–3.
[16] Wang J, Stevens R. Review: zirconia-toughened alumina (ZTA) ceramics. J Mater Sci 1989;24:3421–40.
[17] Mondal B, Chattopadhyay A, Virkar A, Paul A. Development and performance of zirconia-toughened alumina ceramic tools. Wear 1992;156:365–83.
[18] Basu B, Vleugels J, Biest OVD. Toughness tailoring of yttria-doped zirconia ceramics. Mater Sci Eng A 2004;380:215–21.
[19] Magnani G, Brillante A. Effect of the composition and sintering process on mechanical properties and residual stresses in zirconia–alumina composites. J Eur Ceram Soc 2005;25:3383–92.
[20] Huang SG, Vanmeensel K, Biest OVD, Vleugels J. Influence of CeO_2 reduction on the microstructure and mechanical properties of pulsed electric current sintered Y_2O_3–CeO_2 co-stabilized ZrO_2 ceramics. J Am Ceram Soc 2007;90:1420–6.
[21] Sergo V, Vanni L, Giuseppe P, Elio L, Sergoio M, Naoki M, et al. The effect of wear on the tetragonal-to-monoclinic transformation and the residual stress distribution in zirconia-toughened alumina cutting tools. J Wear 1998;214:264–70.
[22] Akin I, Yilmaz E, Sahin F, Yucel O, Goller G. Effect of CeO_2 addition on densification and microstructure of Al_2O_3–YSZ composites. Ceram Int 2011;37:3273–80.
[23] Senthil Kumar A, Raja Durai A, Sornakumar T. Development of yttria and ceria toughened alumina composite for cutting tool application. Int J Refract Metals Hard Mater 2007;25:214–9.
[24] Oh UC, Chung YS, Kim DY, Yoon DN. Effect of grain growth on pore coalescence during the liquid-phase sintering of MgO–$CaMgSiO_4$ systems. J Am Ceram Soc 1988;71:854–7.
[25] German R, editor. Critical reviews in solid state and materials sciences, vol. 35 4. California: Taylor & Francis; 2010.